Resonance Raman Spectra Simulation of the 4,4′-Bipyridine Anion Radical and N-Protonated Radical

Christine Lapouge,* Guy Buntinx, and Olivier Poizat

Laboratoire de Spectrochimie Infrarouge et Raman (LASIR), Centre d'Etude et de Recherches Lasers et Applications, Université de Lille 1, Bâtiment C5, 59655 Villeneuve d'Ascq Cedex, France

Received: October 18, 2001; In Final Form: January 14, 2002

A low-cost computational methodology is utilized to calculate the resonance Raman spectra of the 4,4′-bipyridine anion radical (44BPY$^{-\bullet}$) and *N*-hydro radical (44BPYH$^{\bullet}$). The resonance Raman intensities are evaluated in the Franck−Condon approximation, by projecting the excited state surface gradient (calculated with the CASSCF method) on the ground state normal modes (determined at ROHF level of theory). TD-DFT and CIS calculations are used to assign the resonant electronic states, estimate the intensity and excitation energy of the related transitions, and identify the molecular orbitals involved in these transitions. These molecular orbitals are then used to construct CASSCF active spaces as small as possible and to compute the excited-state gradients. The results appear to be very satisfactory for 44BPY$^{-\bullet}$ and reasonable for 44BPYH$^{\bullet}$. They allow identifying the nature of the probed resonant electronic transitions of these transient species and provide a precise picture of their electronic configuration. A comparative analysis of these results and those reported previously for the lowest excited S_1 state of 44BPY reveals a clear analogy of the electronic structures of the *N*-hydro radical and excited S_1 state.

1. Introduction

Azaaromatic molecules derived from biphenyl have generated great experimental and theoretical interest due to their rich photoreactivity in solution.[1−26] In particular, the combination of transient absorption and time-resolved resonance Raman spectroscopies in the microsecond to picosecond time domain has revealed a powerful method to follow the chemical evolution of the transient species along the photochemical processes. The vibrational data obtained by means of time-resolved resonance Raman spectroscopy have helped in identifying the transient species and sometimes improving the kinetics established from transient absorption, but they have been mainly used to get structural information on these species. In such large molecules for which the normal modes of vibration are described by complex potential energy distributions, the rigorous assignment of the transient state vibrational spectra and their quantitative interpretation in terms of structure require the assistance of theoretical calculations. The approach adopted for this purpose consists of determining the optimized ab initio geometry and then testing the reliability of this geometry by comparing the related theoretical vibrational spectra with the experimental ones. Until now, in most of the investigations, this analysis was essentially based on the comparison of the vibrational wavenumbers of the resonance Raman active modes.

In this respect, particular attention was focused[1−11,15−19,23−25] on the model molecule 4,4′-bipyridine (44BPY) for which the number of totally symmetric, Franck−Condon active modes enhanced in the resonance Raman spectra is low because of a high molecular symmetry. Accordingly, the simplicity of the observed spectra allows an unequivocal correlation between the observed Raman lines and the calculated modes and thus an unambiguous interpretation of the vibrational features. From a theoretical point of view, this model molecule is an ideal subject to test the reliability of the computational method used to simulate the spectra. However, in larger or less symmetric molecules, where a much higher number of vibrations are active in the fingerprint region, the frequency gap between two consecutive modes may be smaller than the precision of the calculation in such a way that the correspondence between experiment and theory is no longer unequivocal. In this case, the predicted ab initio structure cannot be validated only on the basis of the vibrational frequencies and a second experimental basis of comparison is necessary: resonance Raman intensities.

Prediction of resonance Raman intensities has already been the subject of theoretical interest.[27−32] Several methods have been used, more or less sophisticated, but the majority need calculations on resonant excited states such as geometry optimizations or frequency determinations that are not easy to handle for large systems.[28−30] Another approach involves wave packet propagation methods.[31,32]

The purpose of this work is to check to what extent the resonance Raman intensities can be predicted with quite low level ab initio calculations and compared to the experimental features to test the reliability of theoretical structures predicted for transient chemical species. The systems examined here are the anion radical (44BPY$^{-\bullet}$) and *N*-hydro radical (44BPYH$^{\bullet}$) of 4,4′-bipyridine for which the time-resolved resonance Raman frequencies have been clearly interpreted on the basis of quantum calculations.[23,24] In both cases, the Raman intensities are calculated for several isotopomers of 44BPY in resonance with two distinct electronic transitions of the transient species. These data are compared, for the anion radical, with the experimental spectra reported previously[23] and, for the *N*-hydro radical, with new spectra that are presented in parallel.

* To whom correspondence should be addressed. E-mail: Christine.Lapouge@univ-lille1.fr.

10.1021/jp013869s CCC: $22.00
Published on Web 03/30/2002

2. Experimental Section

44BPY was purchased from Aldrich. The 44BPY-d_8 and 44BPY-2,2′,6,6′-d_4 isotopomers were synthesized as reported elsewhere.[23] All samples were sublimed in vacuo prior to each spectroscopic measurement. Methanol (Prolabo) was used as received. Solutions were deoxygenated with an Ar purge directly in the spectroscopic cell. The time-resolved resonance Raman spectra of the photolytically produced *N*-hydro radical species 44BPYH$^{\bullet}$ were obtained by using the nanosecond pump−probe double laser excitation system described previously.[33,34] 44BPYH$^{\bullet}$ was produced by hydrogen atom photoabstraction upon excitation of the parent molecule (10^{-3} M) in methanol with a pump wavelength of 248 nm.[3] Two probe wavelengths of 370 and 532 nm were chosen to excite the Raman spectra in resonance with two distinct electronic transitions of the radical maximizing at 370 and 540 nm, respectively, in alcohols.[1,4,5] The pump−probe delay time was set to 50 ns.

3. Computational Method

The calculation of the resonance Raman intensities was performed by assuming a pure Franck−Condon scattering mechanism.[35,36] This hypothesis is based on the observation that only totally symmetric modes are active in the resonance Raman spectra of the anion radical[23,24] and *N*-hydro radical.[24] In this respect, the global procedure adopted was to project the gradient of the resonant excited state potential surface, determined at the ground state optimized geometry, on the normal modes of the ground state. In fact, in the assumption of harmonic potentials and that no normal mode rotation nor frequency change takes place in the excited state, the relative intensity of a totally symmetric mode q_i is given by[37]

$$I_i \propto \bar{\nu}_i^{-3}(gM^{-1/2}L_i)^2 \qquad (1)$$

where $\bar{\nu}_i$ and L_i are the wavenumber and Cartesian coordinate vector of mode q_i, g is the gradient of the resonant excited state surface at the vertical of the ground state surface minimum, and M is the matrix of atomic masses.

This method has already been used with success in the literature.[27−29]

All ab initio calculations are performed with the Gaussian 98 program.[38] In a previous study focused on the determination of geometric parameters and vibrational frequencies of the 44BPY anion and radical transient species,[24] it has been shown that the 6-31G(+*) basis set, in which polarization and diffuse functions are added only on the nitrogen atoms, is well adapted. In the present work, the 6-31G* basis set, in which polarization functions are added on all C and N atoms but all diffuse functions are removed, is preferred. As a matter of fact, the presence of diffuse functions makes multiconfigurational methods more difficult to employ and increases dramatically the computational cost.

Four levels of ab initio calculations were used in this work as they are implemented in Gaussian 98: ROHF (Restricted Open-shell Hartree−Fock),[39] CIS (Configuration Interaction Singles),[40] CASSCF (Complete Active Space Self-Consistent Field),[41−46] and RPA (Random Phase Approximation).[47] In a first step, geometry optimization and frequency calculations are performed in ROHF for the ground state to obtain normal modes at the minimum of the ground state potential energy surface. Although density functional theory (DFT) would give rise to more accurate results,[24] we used the Hartree−Fock formalism to preserve the same methodology as that employed in the following to determine the gradient of resonant excited states.

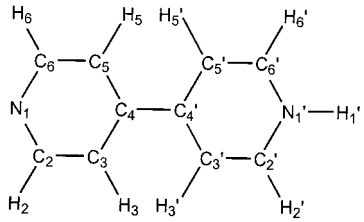

Figure 1. Numbering of the atoms of 44BPY$^{-\bullet}$ and 44BPYH$^{\bullet}$.

In a second step, CIS calculations are carried out to identify the transitions of lowest energies having high transition dipole moments and to determine the molecular orbitals (MOs) implicated in these transitions. Eight excited states were requested for each compound (as many states as symmetry operations[40] in the D_{2h} point group for the anion radical) to ensure a good convergence. The potential surface gradients along all the totally symmetric modes of the ground state species are then calculated for those excited states characterized by allowed transitions and the corresponding resonance Raman intensities are derived from these gradients by using eq 1. In some cases, this level of theory seems to suffice to correctly reproduce resonance Raman spectra.[27]

In parallel, the RPA procedure is used with the B3LYP[48] hybrid functional to get a better prediction of the transition energies, generally more accurately estimated from DFT than from HF methods,[49,50] in order to confirm the previously predicted transitions. Gradients are not calculated in this case because implemented numerical differentiation takes too long to be feasible for the investigated molecules.

Finally, CASSCF calculations are performed to obtain a more accurate estimate of the gradients than from CIS. Active spaces are constructed in such a way that they contain at least the MOs identified from CIS and RPA results for the selected states. They are first deliberately taken as small as possible to reduce the computational time. Then, for each transition, to check the stability of the results, the active space is increased progressively until it incorporates the whole set of MOs of the symmetry species involved in the transition. The results presented in this paper are those obtained with the smallest active space giving rise to a calculated spectrum not significantly different from that obtained with the largest active space. Each CASSCF calculation will be characterized in the following by a term (*n*, *N*), where *n* and *N* are the numbers of electrons and of MOs, respectively, included in the active space.

4. Results and Discussion

A. Anion Radical 44BPY$^{-\bullet}$. From a structural point of view, the geometric parameters of the anion radical have been optimized at the ROHF/6-31G* level and the corresponding bond orders evaluated by the program HONDO[51] from the Gaussian MOs. The geometry is similar to that found previously at the ROHF/3-21G(+*)[23] and B3LYP/6-31G(+*)[24] levels apart from slightly different parameter values, as expected from basis set and methodology effects. It is characterized by a planar, quinoidal-type structure of D_{2h} symmetry, with a notable double bond character of the inter-ring $C_4C_{4'}$ (bond order of 1.29) and ring $C_2C_3/C_{2'}C_{3'}$ bonds (bond order of 1.53) (Figure 1). The scaled vibrational frequencies obtained for the 44BPY$^{-\bullet}$ totally symmetric modes of the three isotopic compounds in the 500−2000 cm^{-1} range are also slightly different from those found previously but still agree with the experimental frequencies observed from time-resolved resonance Raman spectroscopy.[23]

From an electronic point of view, 44BPY$^{-\bullet}$ has been characterized experimentally by two strong UV−visible absorp-

TABLE 1: Characteristics of Excited States of 44BPY$^{-\bullet}$ Calculated from CIS, RPA, and CASSCF Methods: Symmetry of the State, Electronic Transitions Involved, Coefficient of the Configuration in the Wavefunction (*c*), Oscillator Strength (*f*), Excitation Energy (ΔE), and Corresponding Wavelength

D_{2h} point group			CIS				RPA				CASSCF[a]			
state	sym	transition[b]	c[c]	f	ΔE (eV)	λ (nm)	c[c]	f	ΔE (eV)	λ (nm)	active space	MO	ΔE (eV)	λ (nm)
1	B_{2g}	$3b_{3u}^{\alpha} \rightarrow 3b_{2g}^{\alpha}$	0.934	0.4513	3.582	346.1	0.890	0.1413	2.655	467.0	(1, 3)	$3b_{3u}$, $3b_{2g}$, $4b_{2g}$	3.651	339.9
2	B_{2g}	$2b_{2g}^{\beta} \rightarrow 3b_{3u}^{\beta}$	0.848	0.1898	3.855	321.6	0.784	0.4009	3.848	322.1	(3, 3)	$2b_{2g}$, $3b_{3u}$, $4b_{3u}$	4.720	263.0
3	B_{2g}	$1a_{u}^{\beta} \rightarrow 2b_{1g}^{\beta}$	0.468	0.2303	5.343	232.0								
		$1a_{u}^{\alpha} \rightarrow 2b_{1g}^{\alpha}$	0.415											
		$1b_{1g}^{\beta} \rightarrow 2a_{u}^{\beta}$	0.407											

[a] CASSCF active spaces are defined (see text) as well as the molecular orbitals they contain. [b] α and β represent the electron spin. [c] The weight of the configuration in the wave function is equal to c^2. Only coefficients >0.5 are reported.

tion bands peaking at 385 nm and in the 550−600 nm range, respectively,[4,12] revealing the presence of two allowed electronic transitions in the low energy region. The anion radical presents 12 π MOs and 2 n MOs, belonging respectively to the symmetry species b_{2g}, b_{1g}, a_u, and b_{3u} for the first group and a_g and b_{1u} for the second one. They are energetically ordered as in Scheme 1:

Scheme 1

$$1b_{3u}^2\ 1b_{2g}^2\ 2b_{3u}^2\ 10b_{1u}^2\ 11a_g^2\ 1b_{1g}^2\ 1a_u^2\ 2b_{2g}^2\ 3b_{3u}^1\ 2b_{1g}^0\ 3b_{2g}^0\ 2a_u^0\ 4b_{3u}^0\ 4b_{2g}^0$$

The notation $2b_{3u}^2$, for example, designates the second MO of symmetry b_{3u}, doubly occupied in the ground state (exponent 2). From CIS calculations, three excited states give rise to low energy optical transitions with appreciable oscillator strength. The main characteristics predicted for these states are reported in Table 1. They are all of B_{2g} symmetry. The first two correspond to relatively pure one-electron transitions involving the open shell ($3b_{3u}^{\alpha} \rightarrow 3b_{2g}^{\alpha}$ and $2b_{2g}^{\beta} \rightarrow 3b_{3u}^{\beta}$). The last one is a mixing of three configurations with comparable weights that are more energetic and involve orbitals lying deeper in the core compared to the former states. It can be noted that, in all cases, the transitions are of $\pi\pi^*$ type, i.e., the n orbitals do not participate to the excitations.

The results of RPA calculations performed under conditions similar to those of the CIS ones are also shown in Table 1. The two excited states of lowest energies arising from the one-electron $3b_{3u}^{\alpha} \rightarrow 3b_{2g}^{\alpha}$ and $2b_{2g}^{\beta} \rightarrow 3b_{3u}^{\beta}$ transitions (numbered as 1 and 2 in Table 1) are still predicted. The related oscillator strengths are inverted relative to the CIS results but remain strong. The main difference between the results from the two methods is that the excitation energies are more separated and closer to the experimental values in RPA than in CIS. The third CIS transition of high oscillator strength is not calculated at the RPA level. We ascribe thus the absorption bands observed at 385 and 550−600 nm to the one-electron transitions leading to states 1 and 2.

CASSCF calculations are then performed for each transition, with active spaces containing the MOs involved in states 1 and 2. The smallest active spaces giving rise to the same transitions as CIS and RPA calculations and leading to similar relative resonance Raman intensities as the largest ones are given in Table 1. They involve three MOs and one and three electrons respectively for transitions 1 and 2. The weight of the configuration, corresponding to the considered transition, in the excited state wave function is near unity in each case, as expected from the low number of orbitals involved. This weight decreases slightly when opening the active space to other MOs of the same symmetry species, but the one-electron character of the transition is preserved. The CASSCF excitation energies are larger than the RPA ones, but the gap between states 1 and 2 (Table 1) is nearly maintained (1.1 vs 1.2 eV) and remains much larger than in the CIS calculation (0.3 eV). Figure 2A shows a schematic representation of the calculated MOs involved in the two transitions.

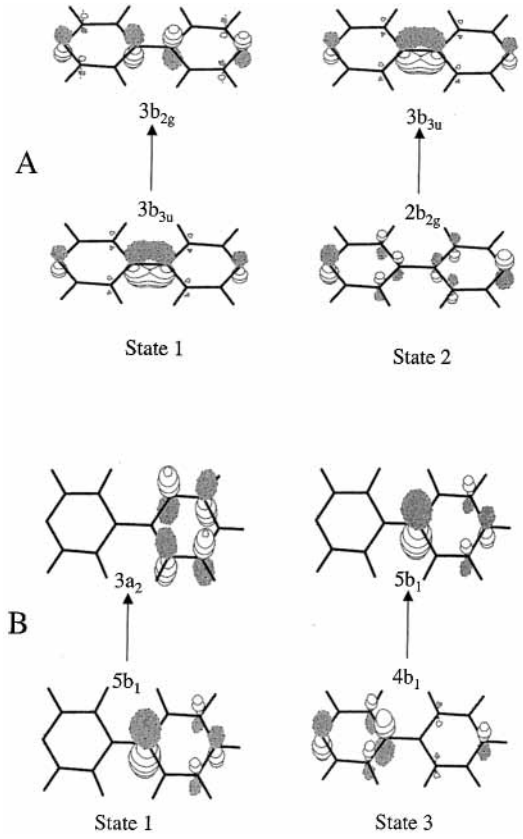

Figure 2. Representation of molecular orbitals involved in (A) transitions of 44BPY$^{-\bullet}$ anion to excited states 1 and 2 (see Table 1) and (B) transitions of 44BPYH$^{\bullet}$ radical to excited states 1 and 3 (see Table 2).

Figure 3 shows the experimental Raman spectra[23] of 44BPY$^{-\bullet}$-h_8 probed in resonance with the 550−600 (λ_{probe} 560 nm) and 385 nm (λ_{probe} 370 nm) absorption bands (parts A and A′, respectively) and the corresponding theoretical spectra calculated in resonance with states 1 and 2 from gradients determined with CASSCF (parts B and B′, respectively) and CIS (parts C and C′, respectively) methods. Figures 4 and 5 show similar results obtained for the 44BPY$^{-\bullet}$-d_4 and 44BPY$^{-\bullet}$-d_8 isotopomers, respectively. The vibrational bands are designated according to the notation of the normal modes established previously[23] from the potential energy distributions

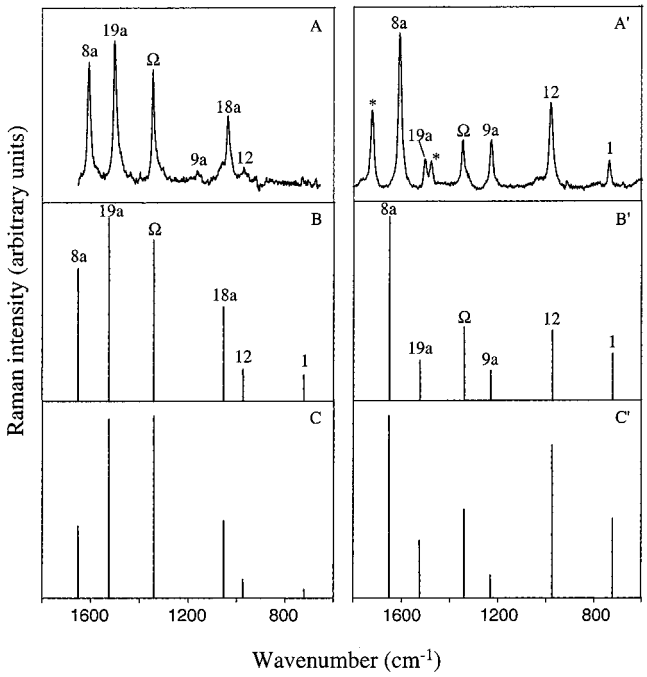

Figure 3. Experimental time-resolved resonance Raman spectra of 44BPY$^{-\bullet}$-h_8 probed at 560 (A) and 370 nm (A′) (from ref 23) and theoretical spectra calculated in resonance with excited states 1 and 2 (see Table 1) from CASSCF (B and B′, respectively) and CIS (C and C′, respectively) gradients. Raman lines marked with the symbol (*) in spectrum A′ are due to harmonic or combination modes. The band notation refers to assignments reported in ref 23.

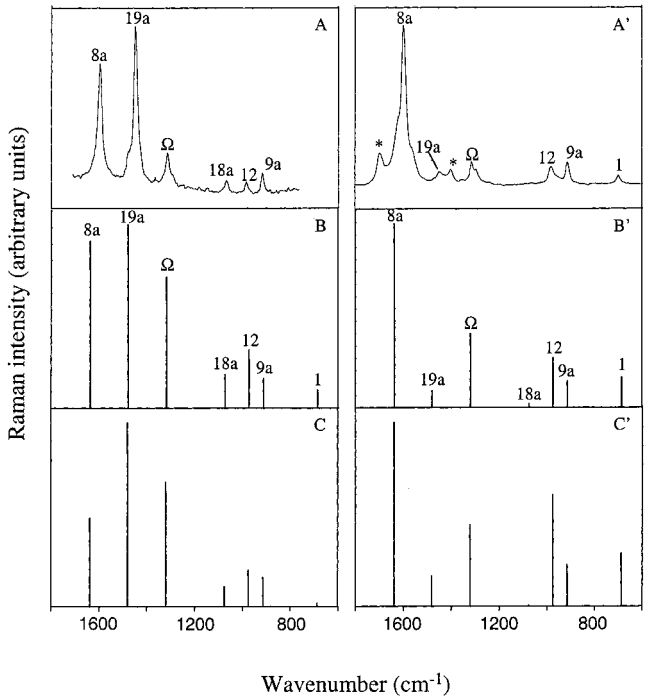

Figure 4. Experimental time-resolved resonance Raman spectra of 44BPY$^{-\bullet}$-d_4 probed at 560 (A) and 370 nm (A′) (from ref 23) and theoretical spectra calculated in resonance with excited states 1 and 2 (see Table 1) from CASSCF (B and B′, respectively) and CIS (C and C′, respectively) gradients. Raman lines marked with the symbol (*) in spectrum A′ are due to harmonic or combination modes. The band notation refers to assignments reported in ref 23.

(PEDs). As already discussed,[23] these bands correspond to the eight totally symmetric modes expected in the fingerprint region 200−1800 cm^{-1} according to the D_{2h} symmetry of the anion radical (in-phase motion of the two rings for each in-plane ring

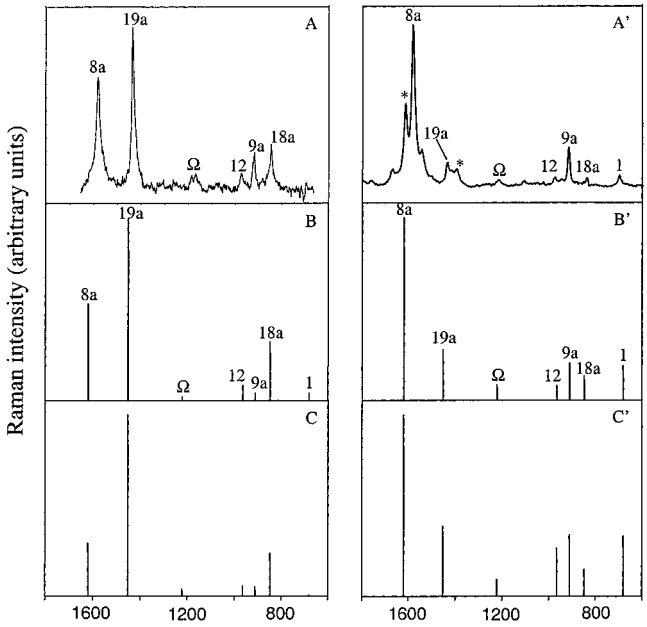

Figure 5. Experimental time-resolved resonance Raman spectra of 44BPY$^{-\bullet}$-d_8 probed at 560 (A) and 370 nm (A′) (from ref 23) and theoretical spectra calculated in resonance with excited states 1 and 2 (see Table 1) from CASSCF (B and B′, respectively) and CIS (C and C′, respectively) gradients. Raman lines marked with the symbol (*) in spectrum A′ are due to harmonic or combination modes. The band notation refers to assignments reported in ref 23.

mode symmetric relative to the long C_2 axis). The first observation is that there is generally good agreement between the experimental and calculated spectra in both transitions. It can also be seen that only minor differences appear between the CASSCF and CIS results.

The main aspect of the 560 nm spectrum observed for the 44BPY$^{-\bullet}$-h_8 species (part A in Figure 3) is the dominant activity of four intense bands at 1612 (ring mode 8a), 1509 (ring mode 19a), 1350 (inter-ring stretching mode Ω), and 1043 cm^{-1} (ring mode 18a), in accord with the calculated spectra (parts B and C). The CASSCF results provide a slightly better simulation of these bands, but the CIS calculations give a more reliable account of the very low intensity observed for the ring modes 1 and 12. The very weak intensity of the 1230 cm^{-1} vibration (ring mode 9a) is well reproduced in both calculations. On the other hand, the 370 nm spectrum of 44BPY$^{-\bullet}$-h_8 (part A′ in Figure 3) is dominated by one intense band at 1612 cm^{-1} (mode 8a) as predicted by the calculations. The intensity enhancement observed for modes 9a, 12, and 1 and the contrasting intensity downfall noted for modes 19a and 18a on going from the 560 to the 370 nm probe excitation are also correctly calculated in the theoretical spectra.

Similar conclusions can be made for the deuterated derivatives (Figures 4 and 5). CASSCF and CIS give comparable profiles, with a better accuracy of the first method in the high frequency range and of the second one in the low frequency range, except for the d_4 isotopomer where the CASSCF spectrum is globally better than the CIS one. Considering the three isotopomers, the agreement between experiment and calculations concerns the following points: the 8a band dominates the 370 nm spectrum; the 19a band dominates the 560 nm spectrum and is much weaker in the 370 nm spectrum; the 1 and 18a bands are stronger upon 370 and 560 nm probing, respectively; mode 6a, expected around 300 cm^{-1}, is never observed; finally, the intensity of the band ascribed to mode Ω decreases progressively on going from the h_8 to the d_4, and then to the d_8 species. As discussed

TABLE 2: Characteristics of Excited States of 44BPYH• in the Symmetry Point Groups C_{2v} and C_2, Calculated from CIS, RPA, and CASSCF Methods: Symmetry of the State, Electronic Transitions Involved, Coefficient of the Configuration in the Wavefunction (c), Oscillator Strength (f), Excitation Energy (ΔE), and Corresponding Wavelength

C_{2v} point group			CIS				RPA				CASSCF[a]				
state	sym	transition[b]	c[c]	f	ΔE (eV)	λ (nm)	c[c]	f	ΔE (eV)	λ (nm)	active space	MO	ΔE(eV)	λ(nm)	f
1	A_2	$5b_1^\alpha \rightarrow 3a_2^\alpha$	0.758	0.0004	3.600	344.4	1.000	0.0004	1.799	689.0	(1, 3)	$5b_1$, $3a_2$, $4a_2$	2.464	503.7	0.0125
		$5b_1^\alpha \rightarrow 4a_2^\alpha$	0.560												
2	B_1	$5b_1^\alpha \rightarrow 6b_1^\alpha$	0.635	0.1060	4.809	257.8	0.878	0.0866	2.855	434.2					
		$4b_1^\beta \rightarrow 5b_1^\beta$					0.505								
3	B_1	$4b_1^\beta \rightarrow 5b_1^\beta$	0.602	0.0798	5.385	230.2	0.679	0.3220	3.905	317.5	(5, 3)	$3b_1$, $4b_1$, $5b_1$	5.107	243.0	0.5941

C_2 point group			CIS				RPA				CASSCF[a]				
state	sym	transition[b]	c[c]	f	ΔE (eV)	λ (nm)	c[c]	f	ΔE (eV)	λ (nm)	active space	MO	ΔE (eV)	λ (nm)	f
1	A	$19b^\alpha \rightarrow 24a^\alpha$	0.758	0.0006	3.572	347.1	1.000	0.0005	1.784	694.9	(1, 3)	19b, 24a, 25a	2.405	516.0	0.0191
		$19b^\alpha \rightarrow 25a^\alpha$	0.562												
2	B	$19b^\alpha \rightarrow 20b^\alpha$	0.640	0.1058	4.846	255.9	0.885	0.0932	2.842	436.2					
3	B	$18b^\beta \rightarrow 19b^\beta$	0.562	0.0658	5.360	231.3	0.682	0.3028	3.908	317.3	(5, 3)	17b, 18b, 19b	4.619	268.7	0.2232

[a] CASSCF active spaces are defined (see text) as well as the molecular orbitals they contain. [b] α and β represent the electron spin. [c] The weight of the configuration in the wave function is equal to c^2. Only coefficients >0.5 are reported.

previously,[23] this intensity evolution upon deuteration parallels a decrease of the contribution of the inter-ring stretching coordinate to the potential energy distribution of this mode. This correlation suggests that the resonance Raman intensity of mode Ω is mainly carried by the inter-ring stretching coordinate (i.e., the resonant excited surface is predominantly displaced along the inter-ring stretching coordinate). It can be noted that the intensity predicted for mode 12 is too intense in the d_4 derivative whereas it appears much more in accord with experiment in the h_8 and d_8 species.

In conclusion, the satisfying prediction of the resonance Raman intensities obtained in the above CASSCF calculations shows that the very restricted active spaces (1, 3) and (3, 3) characterized in Table 1 allow us to correctly describe the excited state curvature (i.e., excited state gradient) at the ground state geometry. This result is interesting since the use of a complete active space with all the n and π orbitals, thus involving a set of 17 electrons in 14 orbitals, would be quasi unrealistic for such a molecule.

It is interesting to note that the transient absorption spectrum observed for 44BPY$^{-\bullet}$ is somewhat similar to that characterizing the anion radical of biphenyl, which presents two strong bands at 625 and 400 nm. These bands have been ascribed from simple molecular orbital considerations to the nearly one-electron excitations $\phi_7 \rightarrow \phi_{10}$ and $\phi_6 \rightarrow \phi_7$ of the biphenyl anion radical.[52,53] From semiempirical calculations, Kihara and Gondo[12] suggested that the 550−600 and 385 nm bands of 44BPY$^{-\bullet}$ derive from these two one-electron transitions, respectively. On the other hand, qualitative analyses of the Raman spectra of 44BPY$^{-\bullet}$ showed[3,12] that the resonance Raman intensities are similar to those observed[54,55] for the biphenyl anion radical and conform to the π-bond order changes expected for these types of excitations. As a confirmation, the quasi one-electron $3b_{3u}^\alpha \rightarrow 3b_{2g}^\alpha$ and $2b_{2g}^\beta \rightarrow 3b_{3u}^\beta$ $\pi\pi^*$ transitions corresponding to the 44BPY$^{-\bullet}$ excited states 1 and 2 in Table 1 are equivalent to the $\phi_7 \rightarrow \phi_{10}$ and $\phi_6 \rightarrow \phi_7$ excitations of the biphenyl anion radical and the ab initio MOs involved in these transitions (Figure 2A) correspond to those expected from the simple Hückel model.[53] The present ab initio calculation confirms thus resolutely the previous analyses of the electronic absorption spectrum of 44BPY$^{-\bullet}$.

B. 44BPYH•. In a previous theoretical investigation at the ROHF/6-31G(+*) level of theory, it was shown[24] that the *N*-hydro radical can be considered as an aromatic pyridyl ring nearly unmodified relative to the parent S_0 molecule, linked to a pyridinium (*N*-monohydropyridyl) ring characterized by a quinoidal type distortion, in an almost planar conformation (inter-ring twist angle of $\sim$11°). The geometric parameters calculated by using the 6-31G* basis set agree with this description, except for the inter-ring twist angle, which reaches a value of 18.5°. The symmetry of the radical, formally C_2, remains close to C_{2v}. The geometric parameters, bond orders, and vibrational frequencies predicted in both cases are not significantly different and do not allow determining the actual symmetry. With respect to this uncertainty, the electronic configuration of the radical was investigated in both the C_{2v} and C_2 hypotheses.

The 44BPYH• radical has been characterized experimentally by two strong absorption bands peaking at 370 nm and in the 540 nm range, respectively,[1,4] indicating, as in the case of the anion radical, the presence of two allowed electronic transitions. 44BPYH• possesses 12 π-type MOs and 1 n-type MO. In the C_{2v} conformation, they belong respectively to the symmetry species b_1 and a_2 for the first group and a_1 for the second one. In C_2 conformation, the distribution is a and b for the π MOs and a for the n MO. They are energetically ordered as in Scheme 2:

Scheme 2

$$1b_1^2\ 2b_1^2\ 3b_1^2\ 21a_1^2\ 1a_2^2\ 4b_1^2\ 2a_2^2\ 5b_1^1\ 3a_2^0\ 6b_1^0\ 4a_2^0\ 7b_1^0\ 8b_1^0\ (C_{2v})$$

$$15b^2\ 16b^2\ 17b^2\ 21a^2\ 22a^2\ 18b^2\ 23a^2\ 19b^1\ 24a^0\ 20b^0\ 25a^0\ 21b^0\ 22b^0\ (C_2)$$

The characteristics of the lowest excited states predicted from CIS calculations are given in Table 2 for the C_{2v} and C_2 point groups. Let us consider first the states numbered 2 and 3 which are predicted to give rise to transitions with important oscillator strengths. These states correspond to the same electronic excitations in C_{2v} and C_2 point groups where both are of B_1 and B symmetry, respectively. State 2 involves, as dominant contribution, the excitation of the lone electron to the first empty b_1 (or b) orbital. Similarly, state 3 arises mainly from the promotion of an electron from the fully occupied b_1 (or b) orbital of highest energy to the open shell. However, these dominant configurations contribute only ca. 60% to the excited state wave functions, which contain also a distribution of weak contribu-

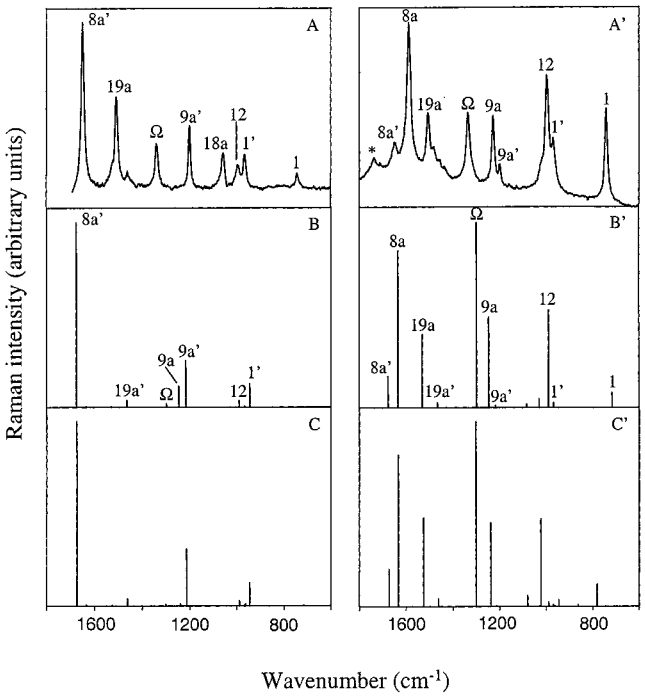

Figure 6. Experimental time-resolved resonance Raman spectra of 44BPYH•-h_8 probed at 532 (A) and 370 nm (A′) and theoretical spectra calculated in resonance with excited states 1 and 3 (see Table 2) from CASSCF gradients in the hypothesis of C_{2v} (B and B′, respectively) and C_2 (C and C′, respectively) symmetry. The Raman line marked with the symbol (*) in spectrum A′ is due to a combination mode. The band notation refers to assignments reported in refs 8 and 24.

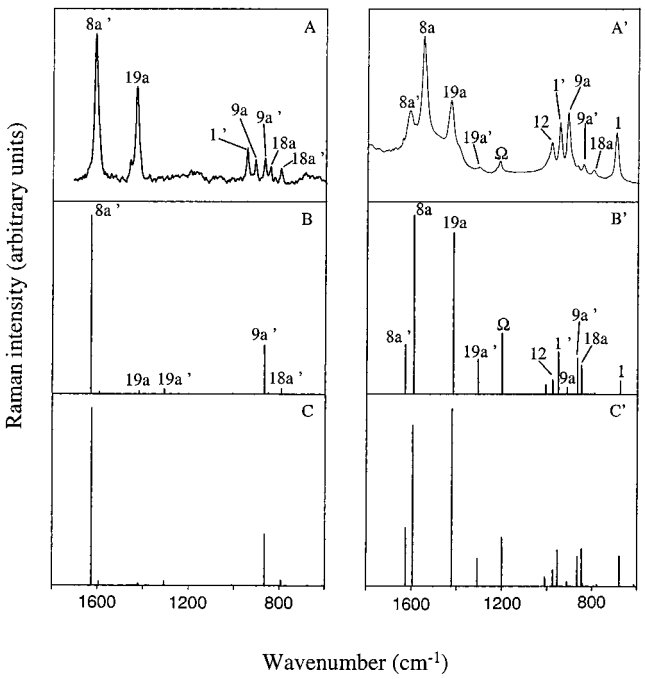

Figure 7. Experimental time-resolved resonance Raman spectra of 44BPYH•-d_8 probed at 532 (A) and 370 nm (A′) and theoretical spectra calculated in resonance with excited states 1 and 3 (see Table 2) from CASSCF gradients in the hypothesis of C_{2v} (B and B′, respectively) and C_2 (C and C′, respectively) symmetry. The band notation refers to assignments reported in refs 8 and 24.

tions from various excitations. Thus, the CIS result suggests that the monoexcited character found in the anion radical transitions is lost for the protonated radical; i.e., the excited states have a marked multiconfigurational character. However, this description of the resonant excited states seems untrustworthy as it leads to simulated Raman spectra (not shown) with relative band intensities in complete disagreement with experiment.

RPA results present the same trends as the CIS ones but predict a higher contribution of the dominant configuration found in each one of the excited states 2 and 3 wave functions and, in state 2, a second important contribution from the same excitation as that calculated for state 3 (in C_{2v} symmetry).

CASSCF calculations were performed to reproduce the different types of transitions identified above for states 2 and 3: the two dominant CIS contributions (e.g., $5b_1^{\alpha} \rightarrow 6b_1^{\alpha}$ and $4b_1^{\beta} \rightarrow 5b_1^{\beta}$ in symmetry C_{2v}) and their combination, as found for state 2 by RPA. For state 3, a monoconfigurational wave function is found with a smallest active space involving five electrons in three orbitals. The theoretical Raman intensities calculated for the 44BPYH•-h_8 and 44BPYH•-d_8 species in resonance with this excited state 3, in both the C_{2v} (part B′ in Figures 6 and 7, respectively) and C_2 (part C′) structure hypotheses, are now in reasonable agreement with the experimental spectra probed at 370 nm (part A′). The UV absorption band observed for the *N*-hydro radical is thus ascribable to an electronic transition to state 3. In contrast, no CASSCF calculation involving the transitions giving rise to state 2 allows a satisfying simulation of the resonance Raman intensities observed in the spectrum probed at 532 nm. This indicates that the *N*-hydro radical absorption band observed in the visible region is likely due to another type of electronic transition. The only possible state predicted from CIS and RPA calculations at low energy is thus that numbered as state 1 in Table 2. This state of A_2 (A) symmetry in the C_{2v} (C_2) hypothesis involves the $5b_1^{\alpha} \rightarrow 3a_2^{\alpha}$ ($19b^{\alpha} \rightarrow 24a^{\alpha}$) transition. The corresponding CASSCF wave function, determined with an active space restricted to one electron and three orbitals, is also essentially described by one singly excited configuration. The corresponding simulated Raman spectra calculated for the 44BPYH•-h_8 and 44BPYH•-d_8 species in the C_{2v} (part B in Figures 6 and 7, respectively) and C_2 (part C) symmetry hypotheses are in better agreement with the experimental spectra probed at 532 nm (part A). A schematic representation of the calculated MOs involved in the transitions to states 1 and 3 are shown in Figure 2B.

The vibrational bands in Figures 6 and 7 are designated by using the notation of the normal modes established previously from the vibrational analysis of the *N*-hydro radical[8] and confirmed by the theoretical PEDs obtained from ab initio calculations.[24] In these investigations, two classes of vibrations were distinguished according to the PEDs. A first group corresponds to ring modes for which the two rings vibrate independently. In this case, for each mode, two localized components denoted *n* and *n*′ characterize the pyridyl and pyridinium rings, respectively (e.g., pairs 8a/8a′ or 9a/9a′). The second group of vibrations are those for which the two rings are largely coupled through the inter-ring stretching motion (Ω). The *n* and *n*′ components are then the in-phase and out-of-phase motions of the two rings (e.g., 1/1′ or 6a/6a′). The Raman modes active in resonance with the UV and visible absorption bands were shown[8,24] to belong exclusively to the 15 totally symmetric modes expected in the region 200−1800 cm^{-1} in the C_{2v} symmetry. We observe in Figures 6 and 7 that the relative Raman intensities calculated in the C_{2v} and C_2 symmetry groups are very similar, which means that the additional totally symmetric modes (out-of-plane ring motions) active in C_2 symmetry are not predicted to give rise to bands with appreciable intensity. This observation indicates that differentiating between

the C_{2v} and C_2 conformations cannot be done on the basis of the resonance Raman intensities.

The simulated spectra in Figures 6 and 7 are not as satisfactory as those found previously for the anion radical. Many discrepancies are observed relative to the experimental spectra. The main disagreements concern modes Ω and 19a, for which the band intensity is predicted too weak in resonance with the visible transition and too intense in resonance with the UV transition. However, some essential features are correctly predicted. One of the most specific resonance effects observed between the experimental spectra probed at 370 and 532 nm (parts A and A′ in Figure 6) is the spectacular intensity inversion characterizing the 8a/8a′ and 9a/9a′ pairs of localized modes. The components localized in the pyridyl moieties are strongly enhanced upon UV excitation, whereas the components localized on the pyridinium moieties are rather enhanced upon visible excitation. These dramatic effects are nicely predicted by the calculation in the C_{2v} (parts B and B′ in Figure 6) and C_2 hypotheses (parts C and C′ in Figure 6). Other points of accord are the notable intensity decrease found for modes 12 and 1 on going from the UV to visible probe excitations. The same trends are found in the case of the d_8 isotopomer (Figure 7). With regard to these analogies between the experimental and calculated spectra, the assignment of the UV and visible electronic absorption bands of the 44BPYH$^{\bullet}$ radical to the transitions to states 3 and 1, respectively, is reasonable.

The last obstacle to ensure these assignments concerns the oscillator strength corresponding to state 1, calculated near zero by both CIS and RPA. Therefore, we used the MOLCAS[56] program to compute it from a CASSCF wave function with active spaces specified in Table 2. Results for states 1 and 3 are reported in the last column. For state 3, the same order of magnitude is retrieved. In contrast, for state 1, values are much greater than those for CIS and RPA, proving the transition is effectively allowed.

The failure of CIS (and maybe RPA) procedure to correctly calculate the transition dipole moment corresponding to state 1 is probably related to the charge transfer character of the transition (Figure 2B). Actually, such a charge displacement implicates an electronic reorganization in σ MOs. This orbital repolarization is not taken into account in CIS where only monoexcitations are involved.

The transitions found for the 44BPYH$^{\bullet}$ radical (Table 2, Figure 2B) differ notably from those characterizing the 44BPY$^{-\bullet}$ anion (Table 1, Figure 2A). Adding a proton to the anion structure does not only induce a slight structural asymmetry of the molecular skeleton as could be expected from the formation of a σ bond from a n orbital, but it also leads to an important redistribution of the π electron configuration resulting in a notable electronic asymmetry. As a consequence, the electronic transition responsible for the visible absorption of the radical species is highly localized in the pyridinium ring, whereas the transition leading to the UV absorption corresponds rather to a charge transfer from the pyridyl to the pyridinium ring. This localized character of the visible transition is consistent with the fact that, for the 8a/8a′ and 9a/9a′ pairs of localized modes, only the intensity of the component characterizing the pyridinium ring is enhanced upon visible excitation. In contrast, according to the representation of the electronic transition calculated for the UV absorption (state 3, Figure 2B), one would expect structural modifications of both the pyridyl and pyridinium rings, and thus notable intensity enhancements for the Raman components of these two rings. Therefore, it is difficult to understand the drastic intensity enhancement inversion observed on going from the visible to the UV excitation, for which only the components localized in the pyridyl moiety are active. This effect reveals the fact that the UV transition leads essentially to an alteration of the geometry of the pyridyl ring. The important point is that the localized character of the resonance Raman intensity enhancements observed upon UV excitation is clearly confirmed by the calculated spectra.

On the other hand, the asymmetry of the π electron distribution of the radical is similar to that found for the lowest excited singlet state, S_1 (nπ^*), where the localized character of the excitation induces a symmetry breaking.[25,26] As a matter of fact, the geometry of the S_1 state (described as an excited nπ^* pyridine substituted with a nearly unperturbated pyridine) presents a clear analogy with the radical structure (a pyridinium radical substituted with a pyridine) since the excited pyridine ring and pyridinium radical ring moieties show comparable distortions.[25] The S_1 state is, as in the case of the *N*-hydro radical, characterized by two absorptions in the UV and visible regions. From ab initio calculations,[26,57] the UV band is assigned to a HOMO → LUMO transition with high charge transfer character from the nonexcited to the excited ring, whereas the visible band involves the π^* electron and leads to a change in electronic density rather localized in the excited pyridyl ring. There is thus an obvious correspondence between the S_1 state transitions and those shown in Figure 2B for the *N*-hydro radical. This analogy of the electronic configuration was suggested from the observation of similar resonance effects in the Raman spectra of the two species.[25,26] It is definitely confirmed by the present work. In particular, the remarkable intensity inversion observed on going from the visible to the UV probe excitation between the two components of some pairs of localized modes such as 8a/8a′ and 9a/9a′ is a common characteristic of the radical and excited S_1 state species. In both cases, the components localized in the perturbed and unperturbed rings are predominantly enhanced in resonance with the visible and UV absorptions, respectively.

5. Conclusion

In this paper, it has been shown that the resonance Raman spectra of transient chemical species of 44BPY can be calculated in a relatively simple way by using ROHF, CIS, TD-DFT (RPA), and CASSCF methods. For the sake of coherence, ROHF allows determining the ground state normal modes with the same methodology as that used in the calculation of the excited state gradient. TD-DFT and CIS provide information on the transition energies, oscillator strengths, and molecular orbitals involved in the transitions. These data are used to construct CASSCF active spaces as small as possible and to calculate the excited state gradients. The resonance Raman intensities are then evaluated, from a simple formula, in the Franck−Condon approximation. This analysis allows identifying the nature of the probed resonant electronic transitions of these transient species and provides a precise picture of their electronic configuration.

For the anion radical, the calculated and experimental spectra obtained in resonance with two distinct electronic absorptions are in good agreement. They confirm the electronic description of the anion proposed from simple molecular orbital considerations. For the *N*-hydro radical, the agreement between theoretical and experimental spectra is not as good as that for the anion radical, probably because of the higher number of active modes and lower molecular symmetry. Nevertheless, the resonant transitions have been identified and an important electronic asymmetry of the two pyridyl rings has been shown, which

appears to be a remarkable characteristic that the radical and the lowest excited S_1 ($n\pi^*$) state of 44BPY have in common.

In conclusion, we can say that the low-cost computational methodology applied to two transient radicals of the test molecule, 4,4′-bipyridine, allows one to obtain very good results concerning the electronic structure of species with high molecular symmetry. When the symmetry decreases, comparison between experimental and theoretical spectra is less satisfying, but general trends are reproduced. Considering the size of the systems studied, the presented low-cost methodology seems promising for further investigations on other similar size or bigger molecules.

Acknowledgment. The authors thank the computing center IDRIS, Orsay, France (Projects 991170, 001170, and 011170) for their help in the development of this work, and CERLA, which is supported by the Ministère Chargé de la Recherche, Région Nord/Pas de Calais, and the Fonds Européen de Développement Economique des Régions. We also thank Dr. J. P. Flament for helpful discussions.

References and Notes

(1) Elisei, F.; Mazzucato, U.; Görner, H.; Schulte-Frohlinde, D. *J. Photochem. Photobiol., A* **1989**, *50A*, 209.

(2) Poizat, O.; Ventura, M.; Buntinx, G. *Spectrosc. Lett.* **1990**, *23*, 701.

(3) Poizat, O.; Buntinx, G.; Ventura, M.; Lautié, M. F. *J Phys. Chem.* **1991**, *95*, 1245.

(4) Buntinx, G.; Valat, P.; Wintgens, V.; Poizat, O. *J. Phys. Chem.* **1991**, *95*, 9347.

(5) Poizat, O.; Buntinx, G.; Valat, P.; Wintgens, V.; Bridoux, M. *J. Phys. Chem.* **1993**, *97*, 5905.

(6) Buntinx, G.; Naskrecki, R.; Poizat, O. *J. Phys. Chem.* **1996**, *100*, 19380.

(7) Didierjean, C.; Buntinx, G.; Poizat, O. *J. Phys. Chem. A* **1998**, *102*, 7938.

(8) Didierjean, C.; DeWaele, V.; Buntinx, G.; Poizat, O. *Chem. Phys.* **1998**, *237*, 169.

(9) Gupta, V. P. *Ind. J. Pure Appl. Phys.* **1973**, *11*, 775.

(10) Sungur, A.; Akyüz, S.; Davies, J. E. D. *J. Inclusion Phenom.* **1987**, *5*, 491.

(11) Topaçli, A.; Akyüz, S. *Spectrochim. Acta* **1995**, *51A*, 633.

(12) Kihara, H.; Gondo, Y. *J. Raman Spectrosc.* **1986**, *17*, 263.

(13) Barker, D. J.; Cooney, R. P.; Summers, L. A. *J. Raman Spectrosc.* **1987**, *18*, 443.

(14) Lu, T.; Cotton, T. M.; Birke, R. L.; Lombardi, J. R. *Langmuir* **1989**, *5*, 406.

(15) Barone, V.; Lelj, F.; Cauletti, C.; Piancastelli, M. N.; Russo, N. *Mol. Phys.* **1983**, *49*, 599.

(16) Barone, V.; Lelj, F.; Commisso, L.; Russo, N.; Cauletti, C.; Piancastelli, M. N. *Chem. Phys.* **1985**, *96*, 435.

(17) Galasso, V.; De Alti, G.; Bigotto, A. *Tetrahedron* **1971**, *27*, 991.

(18) Benedix, R.; Birner, P.; Birnstock, F.; Hennig, H.; Hofmann, H. J. *J. Mol. Struct.* **1979**, *51*, 99.

(19) Bolotin, A. B.; Bolotin, V. A.; Gineityte, V. L. *Int. J. Quantum Chem.* **1979**, *16*, 839.

(20) Hofmann, H. J.; Cimiraglia, R.; Tomasi, J. *J. Mol. Struct. (THEOCHEM)* **1986**, *139*, 213.

(21) Hofmann, H. J.; Cimiraglia, R.; Tomasi, J. *J. Chem. Res., Synop.* **1987**, 48.

(22) Von Nagy-Felsobuki, E. *Chem. Phys. Lett.* **1986**, *127*, 245.

(23) Ould-Moussa, L.; Poizat, O.; Castellà-Ventura, M.; Buntinx, G.; Kassab, E. *J. Phys. Chem.* **1996**, *100*, 2072.

(24) Castellà-Ventura, M.; Kassab, E. *J. Raman Spectrosc.* **1998**, *29*, 511.

(25) DeWaele, V.; Buntinx, G.; Poizat, O.; Flament, J. P.; Kassab, E. *J. Chem. Phys.* **1999**, *110*, 6353.

(26) DeWaele, V.; Buntinx, G.; Poizat, O.; Flament, J. P. *J. Raman Spectrosc.* **2000**, *31*, 275.

(27) Foley, M. S. C.; Braden, D. A.; Hudson, B. S.; Zgierski, M. Z. *J. Phys. Chem. A* **1997**, *101*, 1455.

(28) Peticolas, W. L.; Rush, T., III. *J. Comput. Chem.* **1995**, *16*, 1261.

(29) Negri, F.; Orlandi, G. *J. Mol. Struct.* **2000**, *521*, 197.

(30) Andruniow, T.; Pawlikowski, M. *Chem. Phys. Lett.* **2000**, *321*, 485.

(31) Keszthelyi, T.; Grage, M. M.-L.; Offersgaard, J. F.; Wilbrandt, R.; Svendsen, C.; Mortensen, O. S.; Pedersen, J. K.; Jensen, H. J. Aa. *J. Phys. Chem. A* **2000**, *104*, 2808.

(32) Brouwer, A. M.; Svendsen, C.; Mortensen, O. S.; Wilbrandt, R. *J. Raman Spectrosc.* **1998**, *29*, 439.

(33) Buntinx, G.; Benbouazza, A.; Poizat, O.; Guichard, V. *Chem. Phys. Lett.* **1988**, *153*, 279.

(34) Allet, C.; Buntinx, G.; Locoge-Karbowski, N.; Poizat, O. *J. Phys. IV SC7* **1991**, *1*, 463.

(35) Albrecht, A. C. *J. Chem. Phys.* **1961**, *34*, 1476.

(36) Clark, R. J. H.; Dines, T. J. *Angew. Chem., Int. Ed. Engl.* **1986**, *25*, 131.

(37) Ruschin, S.; Bauer, S. H. *J. Phys. Chem.* **1980**, *84*, 3061.

(38) Frisch, M. J.; Trucks, G. W.; Schlegel, H. B.; Scuseria, G. E.; Robb, M. A.; Cheeseman, J. R.; Zakrzewski, V. G.; Montgomery, J. A., Jr.; Stratmann, R. E.; Burant, J. C.; Dapprich, S.; Millam, J. M.; Daniels, A. D.; Kudin, K. N.; Strain, M. C.; Farkas, O.; Tomasi, J.; Barone, V.; Cossi, M.; Cammi, R.; Mennucci, B.; Pomelli, C.; Adamo, C.; Clifford, S.; Ochterski, J.; Petersson, G. A.; Ayala, P. Y.; Cui, Q.; Morokuma, K.; Malick, D. K.; Rabuck, A. D.; Raghavachari, K.; Foresman, J. B.; Cioslowski, J.; Ortiz, J. V.; Baboul, A. G.; Stefanov, B. B.; Liu, G.; Liashenko, A.; Piskorz, P.; Komaromi, I.; Gomperts, R.; Martin, R. L.; Fox, D. J.; Keith, T.; Al-Laham, M. A.; Peng, C. Y.; Nanayakkara, A.; Challacombe, M.; Gill, P. M. W.; Johnson, B.; Chen, W.; Wong, M. W.; Andres, J. L.; Gonzalez, C.; Head-Gordon, M.; Replogle, E. S.; Pople, J. A. *Gaussian 98*, Revision A.9; Gaussian, Inc.: Pittsburgh, PA, 1998.

(39) McWeeny, R.; Dierksen, G. *J. Chem. Phys.* **1968**, *49*, 4852.

(40) Foresman, J. B.; Head-Gordon, M.; Pople J. A.; Frisch, M. J. *J. Phys. Chem.* **1992**, *96*, 135.

(41) Hegarty, D.; Robb, M. A. *Mol. Phys.* **1979**, *38*, 1795.

(42) Eade, R. H. E.; Robb, M. A. *Chem. Phys. Lett.* **1981**, *83*, 362.

(43) Schlegel, H. B.; Robb, M. A. *Chem. Phys. Lett.* **1982**, *93*, 43.

(44) Bernardi, F.; Bottini, A.; McDougall, J. J. W.; Robb, M. A.; Schlegel, H. B. *Faraday Symp. Chem. Soc.* **1984**, *19*, 137.

(45) Yamamoto, N.; Vreven, T.; Robb, M. A.; Frisch, M. J.; Schlegel, H. B. *Chem. Phys. Lett.* **1996**, *250*, 373.

(46) Frisch, M. J.; Ragazos, I. N.; Robb, M. A.; Schlegel, H. B. *Chem. Phys. Lett.* **1992**, *189*, 524.

(47) Casida, M. E.; Jamorski, C.; Casida, K. C.; Salahub, D. R. *J. Chem. Phys.* **1998**, *108*, 4439.

(48) Becke, A. D. *J. Chem. Phys.* **1993**, *98*, 5648.

(49) Weber, P.; Reimers, J. R. *J. Phys. Chem. A* **1999**, *103*, 9821.

(50) Tozer, D. J.; Handy, N. C. *Phys. Chem. Chem. Phys.* **2000**, *2*, 2117.

(51) Dupuis, M.; Marquez, A.; Davidson, E. R. *HONDO 95.3 from CHEM-Station*; IBM Corporation: Neighborhood Road, Kingston, NY 12401, 1995.

(52) Zahradnik, R.; Carsky, P. *J. Phys. Chem.* **1970**, *74*, 1240.

(53) Matsunuma, S.; Yamaguchi, S.; Hirose, C.; Maeda, S. *J. Phys. Chem.* **1988**, *92*, 1777.

(54) Yamaguchi, S.; Yoshimizu, N.; Maedea, S. *J. Phys. Chem.* **1978**, *82*, 1078.

(55) Aleksandrov, V.; Bobovitch, Y. G.; Maslov, V. G.; Sidorov, A. N. *Opt. Spectrosc.* **1975**, *38*, 387.

(56) Andersson, K.; Blomberg, M. R. A.; Fülscher, M. P.; Karlström, G.; Malmqvist, P.-A.; Neogrady, P.; Olsen, J.; Roos, B. O.; Sadlej, A. J.; Schütz, M.; Seijo, L.; Serrano-Andrès, L.; Siegbahn, P. E. M.; Widmark, P.-O. *MOLCAS*, Version 4; Lund University: Lund, Sweden, 1997.

(57) DeWaele, V. Ph.D. Thesis, University of Lille, France, 1999.